

## RESEARCH ARTICLE

10.1002/2013JC009626

## Special Section:

Western Pacific Ocean Circulation and Climate

## Key Points:

- At least two groups of subthermocline eddy are near the Philippine coast
- Period and principal depth of eddies from the east are about 67 days and 350 m
- Westward eddies are caused by meridional shift of the NEC, NEUC, and topography

## Correspondence to:

T.-L. Chiang,  
tchiangtw@gmail.com

## Citation:

Chiang, T.-L., C.-R. Wu, T. Qu, and Y.-C. Hsin (2015), Activities of 50–80 day subthermocline eddies near the Philippine coast, *J. Geophys. Res. Oceans*, 120, 3606–3623, doi:10.1002/2013JC009626.

Received 18 NOV 2013

Accepted 14 APR 2015

Accepted article online 17 APR 2015

Published online 22 MAY 2015

## Activities of 50–80 day subthermocline eddies near the Philippine coast

Tzu-Ling Chiang<sup>1</sup>, Chau-Ron Wu<sup>1</sup>, Tangdong Qu<sup>2</sup>, and Yi-Chia Hsin<sup>3</sup>

<sup>1</sup>Department of Earth Sciences, National Taiwan Normal University, Taipei, Taiwan, <sup>2</sup>International Pacific Research Center, SOEST, University of Hawaii at Manoa, Honolulu, Hawaii, USA, <sup>3</sup>Research Center for Environmental Changes, Academia Sinica, Taipei, Taiwan

**Abstract** Analyses of outputs from an eddy-resolving ocean general circulation model show that there are at least two groups of subthermocline eddies near the Philippine coast: one originates from the south-east, and the other from the east. The dominant period and principal depth of the former (latter) group of eddies are about 55 days (67 days) and 600 m (350 m), respectively. The propagation speed ( $\sim 0.12 \text{ m s}^{-1}$ ) and diameter ( $\sim 3^\circ$ ) of the two groups of eddies are similar. We suggest that the westward propagating eddies are generated by interactions between meridional movement of the westward-flowing North Equatorial Current, the eastward-flowing North Equatorial Undercurrent, and their interactions with topography. Besides, the analysis indicates that, in comparison with the northwestward propagating subthermocline eddies, the westward propagating ones play a more important role in modulating the subsurface circulation near the Philippine coast.

## 1. Introduction

Eddies are believed to significantly influence the exchange/balance of mass, heat, salt, and primary production, etc. in the global ocean. Eddies also play a key role in climate variability [e.g., Roemmich and Gilson, 2001; Hogg *et al.*, 2008; Qu *et al.*, 2012] and regulate western boundary currents on broad timescales [e.g., Johns *et al.*, 2001; Hsin *et al.*, 2008, 2013; Hsin, 2015]. Roemmich and Gilson [2001] suggested that the eddy variability in the Pacific Subtropical Countercurrent (STCC) region (at  $\sim 22^\circ\text{N}$ ) dominates interannual changes of the equatorward transport of the thermocline and is potentially an important forcing mechanism in the coupled air-sea climate system. Hogg *et al.* [2008] found that eddy heat flux around the Antarctic Circumpolar Current (ACC), energized by increasing wind stress, may be a significant contributor to the warming of the Southern Ocean. In the subsurface, Qu *et al.* [2012] reported the northward intrusion of South Pacific water below and offshore the Mindanao Current (MC) is due to subthermocline eddies. An ensemble of these subthermocline eddies can significantly enhance the northward property flux (fresh water). Therefore, not only eddies near the surface are important, but also the implications of eddies in the subthermocline cannot be ignored.

The southward-flowing Luzon Undercurrent (LUC) and northward-flowing Mindanao Undercurrent (MUC) were found beneath the Kuroshio and MC, respectively, along the Philippine coast (Figure 1) [Hu and Cui, 1989; Hu *et al.*, 1991; Lukas *et al.*, 1991; Qu *et al.*, 1997, 1998; Qu *et al.*, 1999; Wijffels *et al.*, 1995; Hu *et al.*, 2013; Zhang *et al.*, 2014]. Both the LUC and MUC are also considered as important components in large-scale water exchange of the global ocean [e.g., Fine *et al.*, 1994]. By analyzing acoustic Doppler current profile data, Hu *et al.* [2013] reported that the LUC is centered at about 650 m and dominated by intraseasonal variability of 70–80 days. From the result of an eddy-resolving ocean general circulation model (OGCM), Qu *et al.* [2012] proposed that the MUC ranges over the depths of 400–1000 m with high-frequency fluctuations of 50–100 days. By a subsurface mooring at  $\sim 127.05^\circ\text{E}$ ,  $8^\circ\text{N}$ , Zhang *et al.* [2014] reported the northward flow (MUC) is observed below 600 m with intraseasonal variability of 60–80 days. Among others, in the subthermocline off the Philippine coast, Kashino *et al.* [2005] found intraseasonal variations (50–100 days) around 700 m at  $126.7^\circ\text{E}$ ,  $6.8^\circ\text{N}$  by in situ current measurements and thought that the intraseasonal variation below the subsurface layer is associated with ocean eddies in this region. By examining

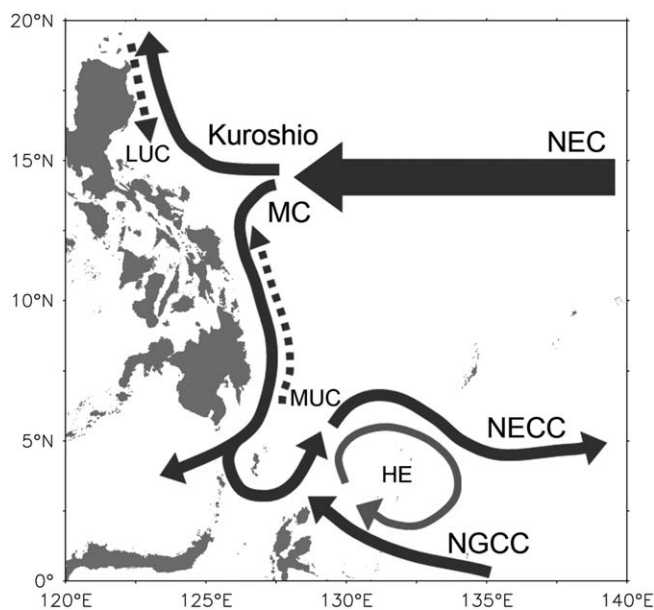


**Figure 1.** Schema of the circulation pattern for the North Equatorial Current (NEC), Kuroshio, Mindanao Current (MC), North Equatorial Countercurrent (NECC), New Guinea Countercurrent (NGCC), Luzon Undercurrent (LUC), Mindanao Undercurrent (MUC), and Halmahera Eddy (HE). The solid and dotted arrows denote the surface and subsurface currents, respectively.

results of an eddy-resolving OGCM, *Chiang and Qu* [2013] also found considerably intraseasonal variabilities existing in the subthermocline of the western equatorial Pacific and further ascribed these intraseasonal variabilities to the impinging of subthermocline eddies.

Recently, there are some observational studies showing the eddies exist in the subthermocline off east Mindanao in the Philippine Sea [e.g., *Wijffels et al.*, 1995; *Kashino et al.*, 1999; *Firing et al.*, 2005; *Kashino et al.*, 2005]. These subthermocline eddies are mostly invisible at the sea surface but may significantly affect the ocean property transports [*Firing et al.*, 2005]. Although information about the subthermocline circulation is still fragmentary, subthermocline eddies have been extensively observed and investigated in several parts of the global ocean [e.g., *Firing et al.*, 2005; *Johnson and McTaggart*, 2010; *Kashino et al.*, 1999, 2005; *Richardson et al.*, 2000; *Shapiro and Meschanov*, 1991; *Simpson and Lynn*, 1990; *Wijffels et al.*, 1995].

By analyzing outcomes of an eddy-resolving OGCM, *Qu et al.* [2012] concluded that the northward intrusion of the South Pacific water below and offshore the MC is largely associated with subthermocline eddies. An ensemble of these subthermocline eddies can significantly enhance the northward property flux, explaining why the water of the South Pacific origin appears to extend farther northward than the mean current there.

To date, our understanding of subthermocline eddies off the Philippine coast is incomplete. A complete description of these subthermocline eddy activities is still lacking. This is due to spatial and temporal limitations of in situ observations in the subsurface. The goal of this study is to investigate the general behavior of subthermocline eddies near the Philippine coast by analyzing results from the eddy-resolving OGCM for the Earth Simulator (OFES). Based on the analyses, we find the high eddy kinetic energy in the subsurface layer near the Philippine coast is mainly contributed from two groups of subthermocline eddies on the timescales of 50–80 days. Two issues are further addressed in this study. The first is to clarify what activities of the two groups near the Philippine coast are, and the second is to identify the relative importance of them. The rest of the paper is structured as follows. Section 2 describes the OGCM used for the present study. In section 3, the general circulation and its variation off east Philippines simulated by the model are presented. The properties, activities, and possible mechanism concerning the subthermocline eddies are explored in details in section 4. Summary and discussion are provided in section 5.

## 2. Model Description

Based on the Modular Ocean Model version 3 (MOM-3.0), the OFES is established in a near-global domain extending from 75°S to 75°N. The OFES has a horizontal resolution of  $0.1^\circ \times 0.1^\circ$  and 54 levels in vertical with variable thicknesses from 5 m near the surface to 330 m near the bottom. The bottom topography of the OFES was derived from a  $1/30^\circ$  bathymetry data set compiled by the Ocean Circulation and Climate Advanced Modeling project (OCCAM) at the Southampton Oceanography Center. Initialized from annual mean fields of temperature and salinity of the World Ocean Atlas (WOA98), the model was first spun up for 50 years. The model was sequentially driven by daily surface wind stress, heat flux, and salinity flux for the period from 1950 to 2009. These daily surface fluxes were provided by the National Centers for

Environmental Prediction (NCEP) reanalysis products. In addition that surface fluxes were specified from reanalyzed atmospheric variables of the NCEP with bulk formula, the surface salinity was restored to climatological monthly values of the WOA98. The snapshotted model outputs, including velocity, temperature, and salinity, were saved at an interval of 3 days. The outputs in the period of 1980–2009 (30 years) are used in the present study. For details about the model configuration, the readers are referred to *Masumoto et al.* [2004] and *Sasaki et al.* [2008].

The OFES outputs have been extensively analyzed by a number of earlier studies for variable areas [e.g., *Sasai et al.*, 2004; *Du et al.*, 2005; *Nakamura and Kagimoto*, 2006; *Qu et al.*, 2008; *Dutrieux*, 2009; *Kashino et al.*, 2009; *Qu et al.*, 2012; *Chiang and Qu*, 2013; *Qiu et al.*, 2013a]. These studies evidenced that the model can reproduce nearly all the observed features over the global ocean. In the far western tropical Pacific, *Dutrieux* [2009] made a comparison between model results and available shipboard acoustic Doppler current profiler (SADCP) measurements, and found that the regional circulation and its variability are well represented by the OFES. Comparing model simulations with mooring data off the northern New Guinea coast, *Chiang and Qu* [2013] also showed good performance of the model for both the surface (upper 200 m) and subsurface (500–1000 m) in the area studied. Based on these studies, we believe that the circulation simulated by the OFES is one of the best available in a model and its outcomes presented in this study are mostly reliable.

### 3. General Circulation and its Variation off East Philippines

As shown in the modeled mean flow at the depth of 108 m in the western equatorial Pacific Ocean (Figure 2a), the North Equatorial Current (NEC;  $\sim 0.125 \text{ m s}^{-1}$ ) ranges over the latitudes of  $8^\circ\text{N}$ – $18^\circ\text{N}$  and flows westward to the Philippine coast. The NEC splits into the northward-flowing Kuroshio and southward-flowing MC at  $\sim 15^\circ\text{N}$  near the Philippine coast, showing a reasonable agreement with earlier studies (Figure 1) [e.g., *Nitani*, 1972; *Toole et al.*, 1990; *Qu and Lukas*, 2003; *Yaremchuk and Qu*, 2004]. After bifurcating, the mean MC reaches the maximum strength ( $\sim 1.3 \text{ m s}^{-1}$ ) near  $7^\circ\text{N}$ . Afterward, a part of the MC enters the Celebes Sea, and the rest turns eastward to feed the eastward-flowing North Equatorial Countercurrent (NECC). West of  $\sim 135^\circ\text{E}$ , the eastward NECC to the north and the westward New Guinea Coastal Current to the south form an anticyclonic eddy, the so-called Halmahera Eddy (HE) (Figure 1) [*Wyrтки*, 1961]. At the depth of 108 m (Figure 2b), the standard deviations (STD) along the coast are relatively low in the Kuroshio and MC region compared with the mean values. In the western equatorial Pacific, the largest STD occurs in the NECC region but is still lower compared with its mean value, whereas the STD in the NEC region is of the same order as the mean flow.

The mean flow and its variations at 358 m (Figures 2c and 2d) are distinct from those at the surface. The NEC at this depth is weaker ( $\sim 0.06 \text{ m s}^{-1}$ ) than that at the surface. It is located north of  $\sim 12^\circ\text{N}$  with a central position at  $17^\circ\text{N}$ – $18^\circ\text{N}$ , indicating a northward movement with increasing depth, in a good agreement with the past studies [e.g., *Qu and Lukas*, 2003; *Kim et al.*, 2004]. The MC and NECC east of  $\sim 132^\circ\text{E}$  become weaker and narrower at this depth, and the NECC moves significantly to the south [*Qiu et al.*, 2013a]. Between the MC and NECC is the anticyclonic HE, showing a poleward tilt of the HE with depth. Such a poleward tilt has been suggested by *Qu et al.* [1999] and observed by *Kashino et al.* [2013]. Unlike the situation at the surface, the STD at the depth of 358 m (Figure 2d) is more significant, especially in the longitude band of  $8^\circ\text{N}$ – $12^\circ\text{N}$  off the Philippines, where the STD ( $\sim 0.12 \text{ m s}^{-1}$ ) is about 6 times larger than the mean velocity ( $\sim 0.02 \text{ m s}^{-1}$ ). At deeper depth of 605 m (Figure 2e), the flow field changes more/less in the north/south of  $\sim 7^\circ\text{N}$ . The NEC and MC are nearly invisible. The distribution of STD at this depth (Figure 2f) is similar to that at 358m. Higher STD still takes place at  $8^\circ\text{N}$ – $12^\circ\text{N}$  off the Philippine coast.

### 4. Eddy Kinetic Energy in the Subthermocline off East Philippines

Eddy kinetic energy (EKE) is a commonly used property for ocean research [e.g., *Qiu*, 1999; *Chiang and Qu*, 2013]. The EKE (per unit mass) is computed as

$$EKE = EKE_z + EKE_M = \frac{1}{2} \langle U'^2 \rangle + \frac{1}{2} \langle V'^2 \rangle, \quad (1)$$

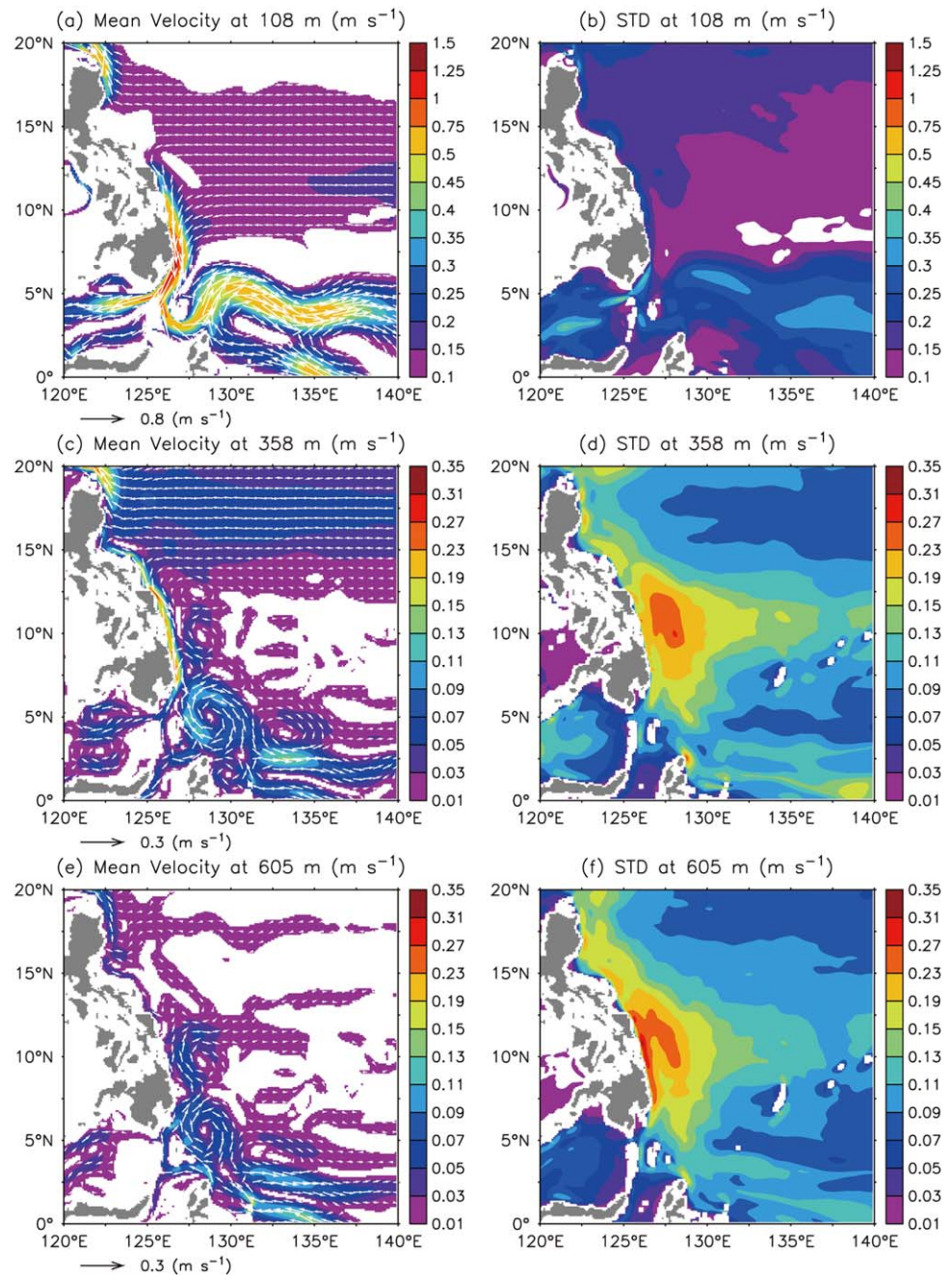


**Figure 2.** Mean (left) and STD (right) of the modeled velocity at the depths of (a, b) 108, (c, d) 358, and (e, f) 605 m. Shading in the left plots indicates the magnitude of velocity.

where  $EKE_Z = \frac{1}{2} \langle U'^2 \rangle$  and  $EKE_M = \frac{1}{2} \langle V'^2 \rangle$  are the zonal and meridional components of EKE,  $U'$  and  $V'$  are the zonal and meridional velocity anomalies, and  $\langle . \rangle$  denotes the time average from 1980 to 2009. If eddies prevalingly propagate along a fixed trajectory, two energetic bands of the along-trajectory component of EKE may be formed on two sides of the trajectory, and one energetic band of the cross-trajectory component of EKE may be generated between the two along-trajectory bands [Chiang and Qu, 2013]. In specific, if eddies mainly propagate in a north-south path, two energetic bands may be shown in the  $EKE_M$  map and one energetic band may be shown in the  $EKE_Z$  map.

The EKEs at the depths of 358 and 605 m are shown in Figures 3a and 3b, respectively. Higher EKE values are present along the Philippine and New Guinea coasts at both depths, indicating high eddy

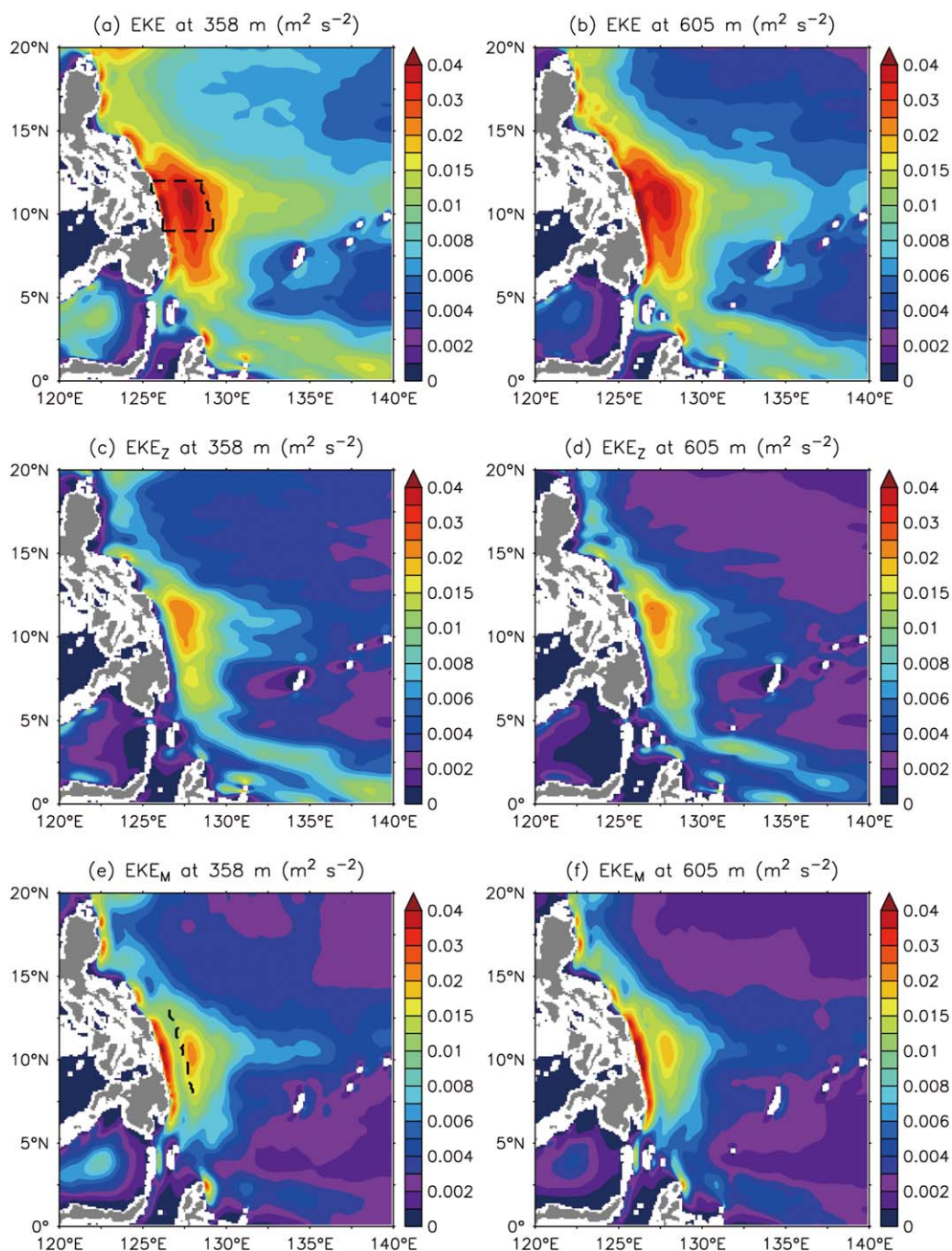


**Figure 3.** Modeled (a, b) total (EKE), (c, d) zonal component ( $EKE_z$ ), and (e, f) meridional ( $EKE_M$ ) component of eddy kinetic energy at the depths of 358 m (left plots) and 605 m (right plots). The dashed frame in Figure 3a and dashed line in Figure 3e indicate the area three degrees away from the coast and  $9^{\circ}N$ – $12^{\circ}N$  for Table 1 and the section along the coast for Figure 15a, respectively.

activities in the subthermocline. Zonal and meridional EKE components ( $EKE_z$  and  $EKE_M$ ) are visible in Figures 3c–3f. Two high  $EKE_z$  ( $>0.005 m^2 s^{-2}$ ) bands (Figures 3c and 3d) and one high  $EKE_M$  band (Figures 3e and 3f) appear along the New Guinea coast ( $127^{\circ}E$ – $140^{\circ}E$ ,  $0^{\circ}$ – $5^{\circ}N$ ), indicative of a northwest-southeast dominant pathway of subthermocline eddies there. Moreover, two high  $EKE_z$  ( $>0.005 m^2 s^{-2}$ ) bands (Figures 3c and 3d) and one high  $EKE_M$  band (Figures 3e and 3f) appear across the Philippine coast ( $126^{\circ}E$ – $137^{\circ}E$ ,  $9^{\circ}N$ – $12^{\circ}N$ ), showing an east-west dominant pathway of subthermocline eddies. The activities of east-westward-propagating eddies are more energetic at 358 m than

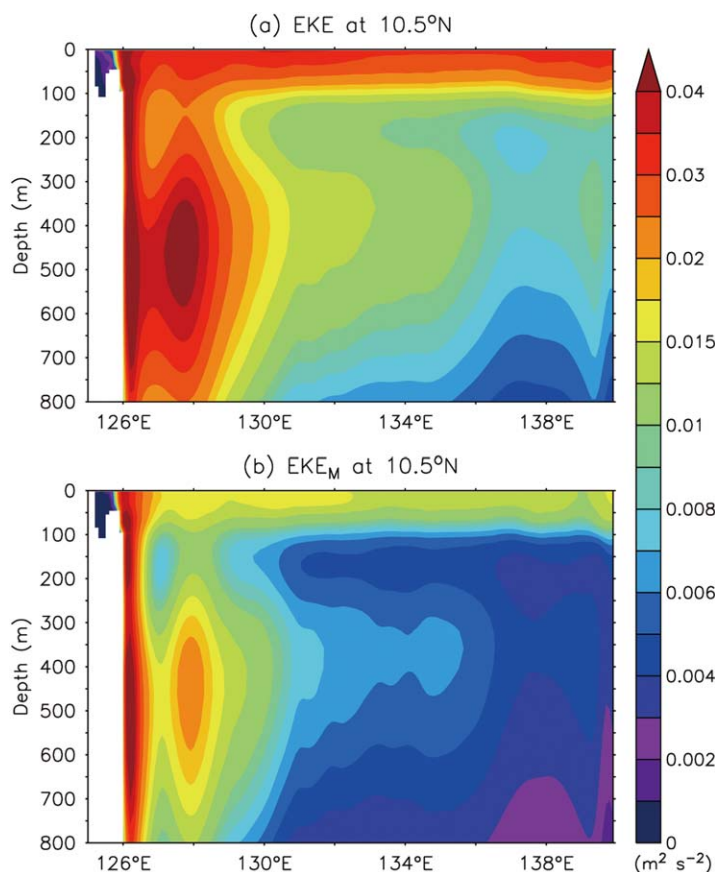


**Figure 4.** Longitude-depth section profiles of (a) EKE and (b) EKE<sub>M</sub> along 10.5°N.

those at 605m. In sum, two groups of subthermocline eddies impinge the Philippine coast and cause higher EKE values there. One is the northwest-southeast moving eddies extending southward to the equator, and the other is the east-west moving eddies centered at  $\sim 10.5^\circ\text{N}$  that extend eastward to  $\sim 136^\circ\text{E}$ . As a result of interaction between eddies and boundary topography, the EKE is accumulated to be the highest along the Philippine coast ( $125^\circ\text{E}$ – $130^\circ\text{E}$ ,  $5^\circ\text{N}$ – $15^\circ\text{N}$ ). Other mechanisms, such as instability induced by variation of currents and local bottom topography, can also contribute some energies to the high EKE [e.g., Bracco *et al.*, 2008].

#### 4.1. Northwestward Propagating Eddies

Firing *et al.* [2005] proposed that the subthermocline flow off the Philippine coast is part of an energetic set of eddies within 300 km of the coast,

and suspected that these eddies represent energy that has propagated along the coast and/or westward and downward. Chiang and Qu [2013] suggested that some of subthermocline eddies propagating in the northwest-southeast direction along the coast originate from the equatorial South Pacific Ocean. These eddies propagate northwestward along the New Guinea coast, cross the equator, and reach the Mindanao coast. The generation of these northwestward-propagating eddies is due in a large part to interactions among the New Guinea Coastal Undercurrent, Lower Equatorial Intermediate Current, and complex topography associated with the Ninigo Group. By analyzing the OFES model results, they also found that the principal depth of these eddies is around 600 m, the dominant timescale is 50–60 days, and the typical propagation speed is  $\sim 0.12 \text{ m s}^{-1}$ .

#### 4.2. Westward Propagating Eddies

##### 4.2.1. Properties

Since the group of east-west moving eddies is centered around the latitude of  $10.5^\circ\text{N}$  (Figure 3), vertical profiles of EKE and EKE<sub>M</sub> at  $10.5^\circ\text{N}$  are shown in Figure 4 to examine the vertical distribution of energy induced by east-west moving eddies. The EKE can be generally divided vertically into three layers: upper 100 m, 100–200 m, and below 200 m. In the upper 100 m, high EKE extends from the Philippine coast to east of  $140^\circ\text{E}$  (the east bound of the map). This high EKE could be induced by high-frequency fluctuations of the atmosphere or by the instability in the interior ocean. Between 100 and 200 m, the level of EKE is lower besides the coast area. Below 200 m, both EKE and EKE<sub>M</sub> show a propagating signal from  $\sim 136^\circ\text{E}$  to the western boundary. In vertical, these eddies have a broad depth range of 200–600 m but most of them are confined between 300 and 400 m.

Figure 5a shows the power spectral density (PSD) of the meridional velocity ( $V$ ) at the depth of 358 m along  $10.5^\circ\text{N}$ . The high PSD in the area three degrees away from the coast (west of  $129^\circ\text{E}$ ) is dominated by a broad range of intraseasonal signals from 50 to 180 days. These intraseasonal signals result from the interaction

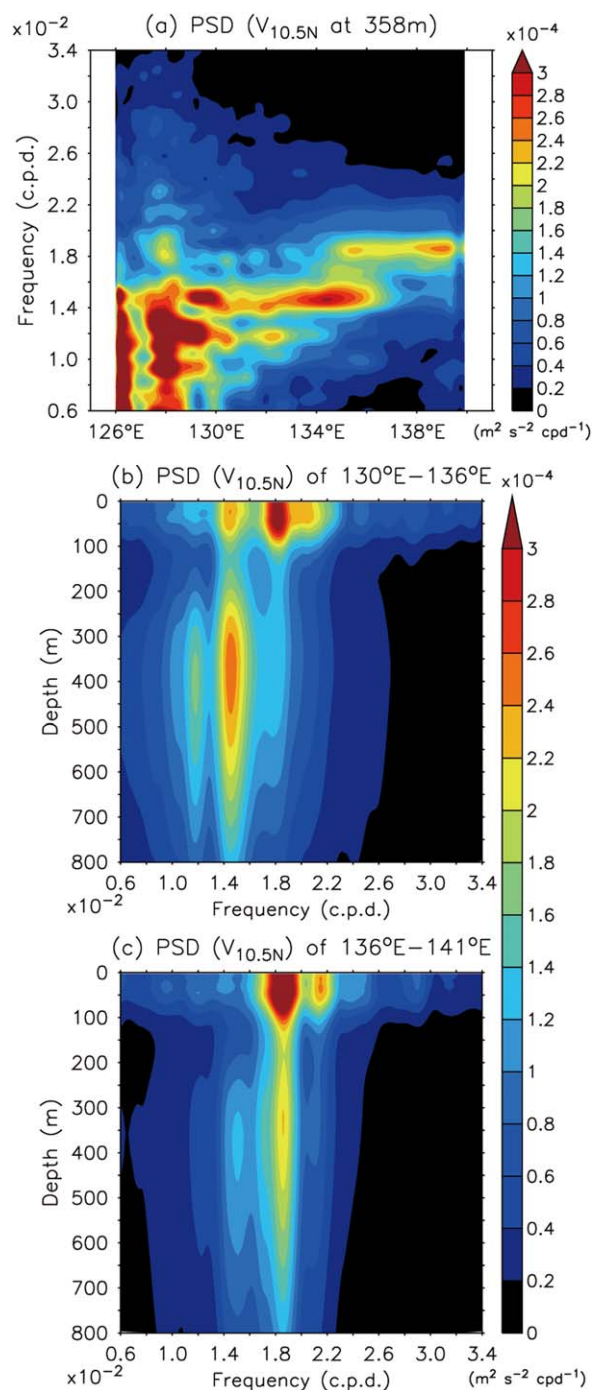


**Figure 5.** (a) Longitude-dependent power spectral density (PSD) at the depth of 358 m, and z-dependent PSD of the meridional velocity (V) averaged over (b) 130°E–136°E and (c) 136°E–141°E. All PSD are derived from the V at 10.5°N.

Similar result is also demonstrated in the lag correlation maps (Figure 8) of 62–72 day band passed relative vorticity (RV) at 358 m relative to the RV at 130°E, 10.5°N. The above outcome suggests that most subthermocline eddies on the timescale of  $\sim 67$  days off the Philippine coast originate near 137°E and propagate westward.

To demonstrate the existence of westward propagating eddies, an Empirical Orthogonal Function (EOF) analysis is applied to the time series of vertical profile of V along 10.5°N. Based on the vertical distribution of EKE along 10.5°N (Figure 4), the domain of the analysis is chosen at 129.5°E–136.5°E

between lateral land boundary and eddies or currents (MC or MUC) [Bracco *et al.*, 2008; Chiang and Qu, 2013]. In addition, the PSD is dominated by fluctuations on the timescales of 62–72 days and 50–60 days in the west and east of 136°E, respectively. Because of this discrepancy, the z-dependent PSD of V at 10.5°N averaged over 130°E–136°E and 136°E–141°E are presented in Figures 5b and 5c to further examine the vertical distribution of eddy activities in the west and east of 136°E. Between 130°E and 136°E, the signal of  $\sim 67$  days is evident in the upper 100 m and 200–600 m layers, but the signal of  $\sim 55$  days is prominent only in the upper 100 m (Figure 5b). Different PSD pattern is shown in the east of 136°E (Figure 5c), where the PSD is dominated by the 55 day signal in the whole depth above 800 m.

Figure 6 presents the PSD profile of V on the period of 67 days along 10.5°N and its phase at 358 m. The 67 day signal initializes near 136°E around 350 m and propagates to the west afterward. Based on the Fast Fourier Transform, the phase of the 67 day signal indicates that the typical propagation speed of this signal is about  $0.12 m s^{-1}$  westward (Figure 6b). Using V at (130°E, 10.5°N, 358 m) as a reference, the coherence spectral analyses are performed with V at different locations (128, 134, 135, 136, 137, and 138°E) along 10.5°N at the same depth of 358 m to trace the origin of the 67 day signal (Figure 7). The squared coherence decreases to the east, and a significant coherence at  $\sim 67$  days is shown in regions west of 137°E, providing additional evidence that the 67 day signal originates around 136°E–137°E along 10.5°N. Besides, Figure 7a (128°E) also shows a high coherence occurring at the signal of  $\sim 67$  days, evidencing clearly that the westward propagating eddies can reach west of 130°E.

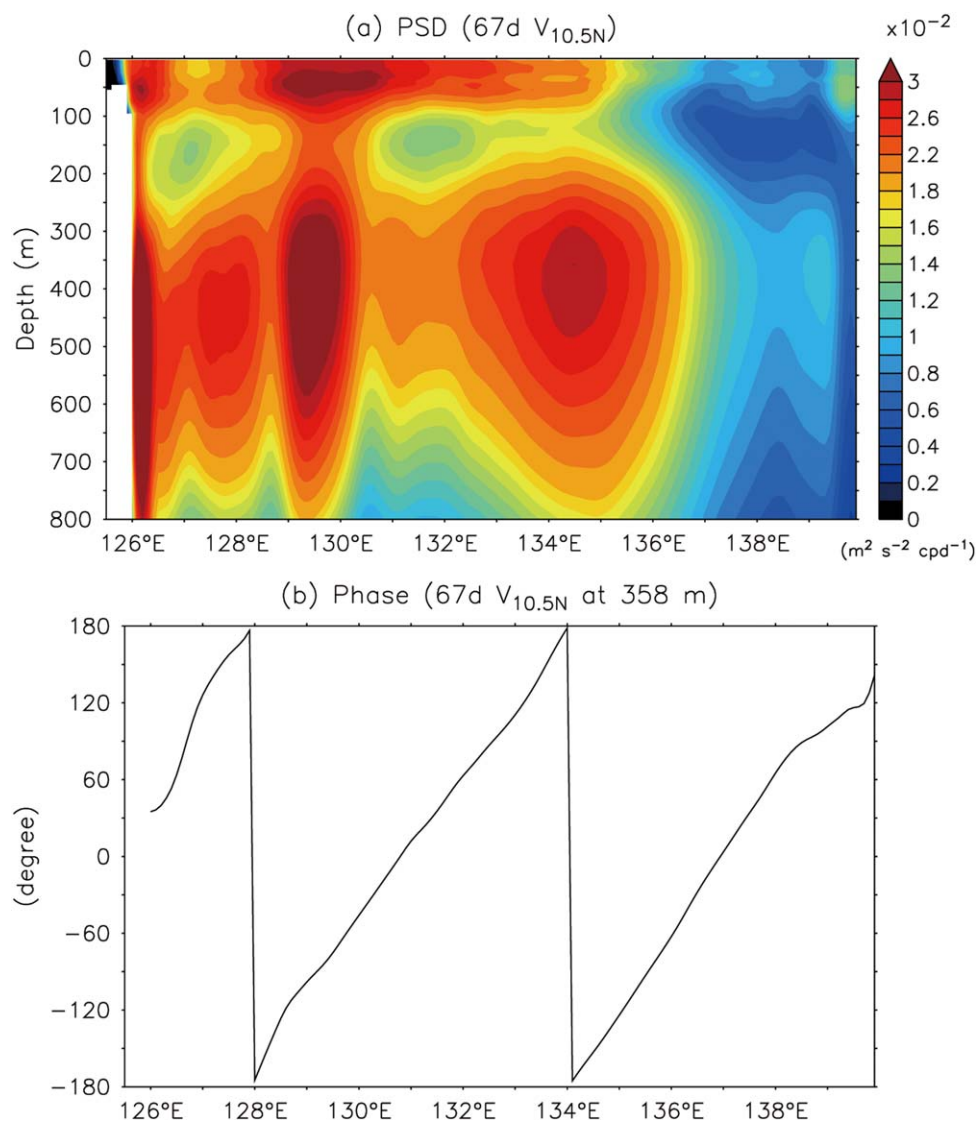


**Figure 6.** (a) Vertical PSD distribution of  $V$  at  $10.5^\circ N$  on the period of 67 days, and (b) the corresponding phase at the depth of 358 m.

zonally and 200–800 m vertically. Before executing the EOF analysis, a 30 day low pass filter is first applied to remove fluctuations on timescales shorter than 1 month. The first and second EOF modes capture about 29% and 26% of the total variance, respectively (Figures 9a and 9b). Not only percentages of the two leading modes explain a similar amount of the total variance, but also spatial pattern and time series of the two modes look very much alike. The time series of mode 2 leads that of mode 1 by 15 days, and the two modes have a correlation coefficient of 0.87. Moreover, the spectra of both PCs peak at  $\sim 67$  days (Figure 9c). Those features imply that the two modes appear to form a propagating signal in the vertical profile of  $V$ .

Extreme variabilities are found in spatial patterns of the two leading EOF modes at 300–400 m. The distance between maximum (red) and minimum (blue) values is about  $3^\circ$ , suggesting a radius of about  $1.5^\circ$ . The node (white) between maximum and minimum values is regarded as the center of subthermocline eddies. With the second mode leading the first mode by 15 days, the two modes have a good correlation. This implies that, when considering a positive value in the west and negative value in the east, a clockwise eddy moves from  $\sim 132.6^\circ E$  (the second mode) westward to  $\sim 131.1^\circ E$  (the first mode) in 15 days. According to the propagating signal of the two modes, the speed of subthermocline eddies is estimated at  $\sim 0.13 m s^{-1}$  ( $1.5^\circ/15 d$ ).

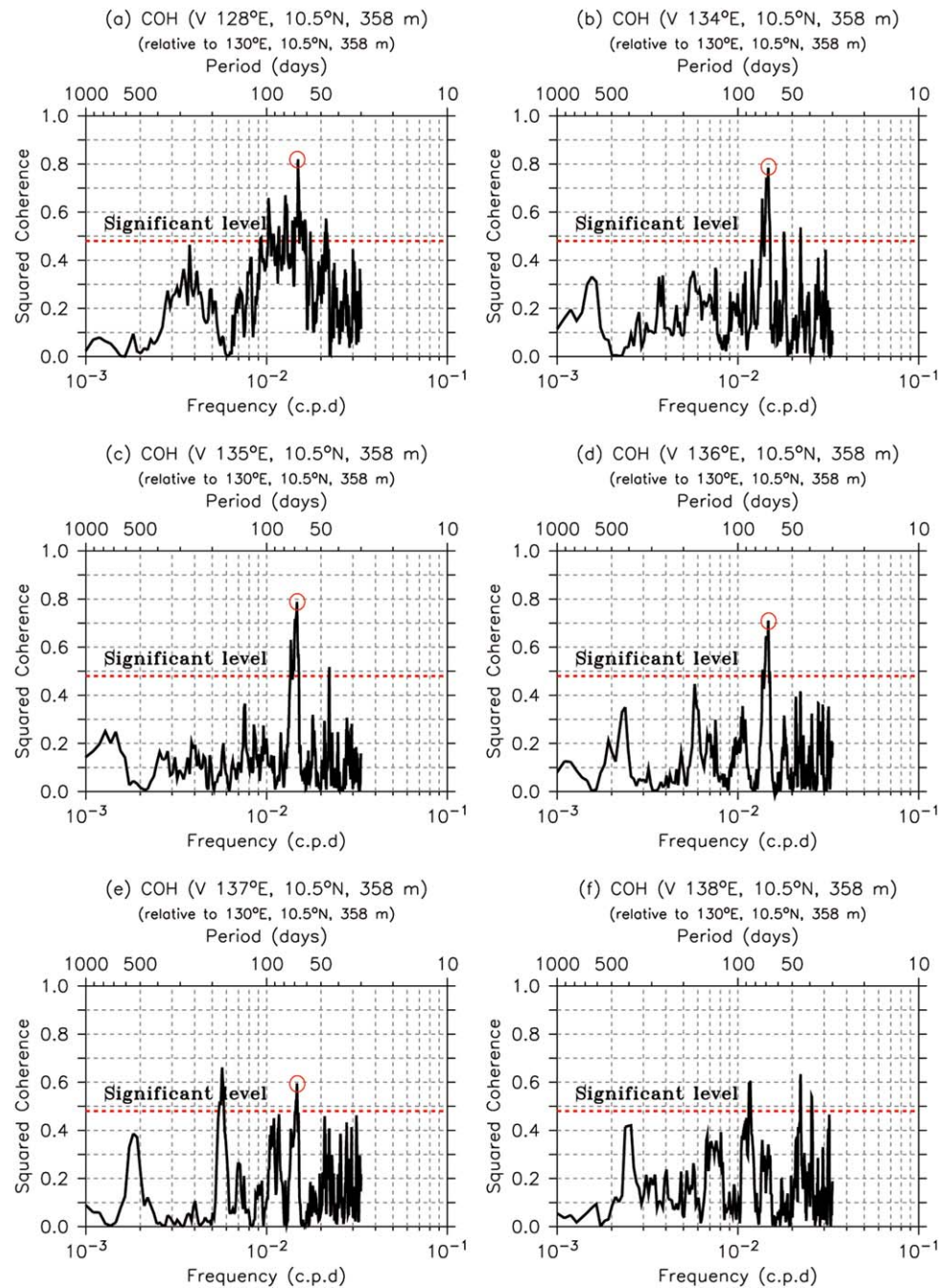


**Figure 7.** Squared coherence spectra of V at the depth of 358m for the locations of (a) 128, (b) 134, (c) 135, (d) 136, (e) 137, and (f) 138°E along 10.5°N relative to the point of 130°E, 10.5°N. The dotted line denotes the 95% significant level.

**4.2.2. Possible Mechanism**

Figure 10 shows flow fields at 54, 148, and 358 m, based on the vertical distribution of EKE in Figure 4. Between 8°N and 12°N, the flow pattern is dominated by a westward current, the NEC, at the two upper layers (Figures 10a and 10b), whereas it is dominated by an eastward current at the lower layer (Figure 10c). This kind of vertical distribution has been shown in the literature [Qiu and Joyce, 1992; Cravatte et al., 2012; Qiu et al., 2013b]. Qiu et al. [2013b] found that an eastward-flowing current, named the North Equatorial Undercurrent (NEUC), takes place below the NEC with a core velocity of 0.02–0.05 m s<sup>-1</sup>. Qiu et al. [2013a] further suggested that the NEUC is formed by converging potential vorticity fluxes. As shown in Figure 10c,

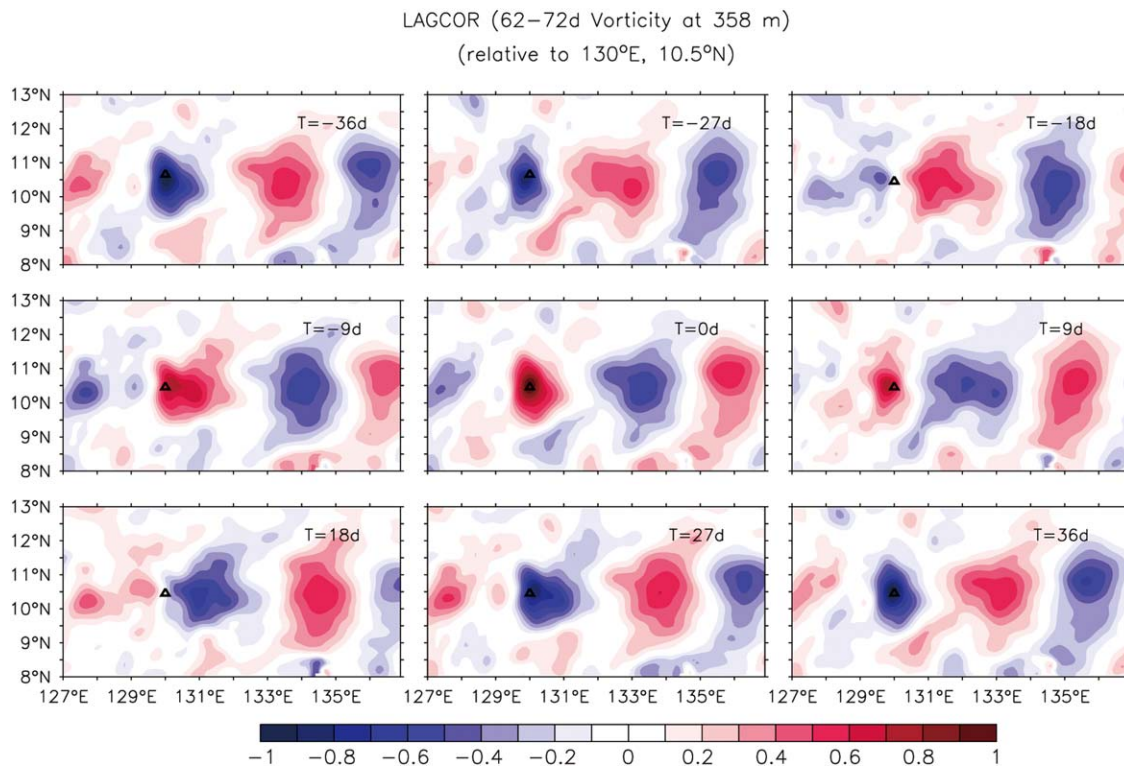


**Figure 8.** Lag correlation maps of 62–72 day band passed relative vorticity (RV) at 358 m relative to the RV at 130°E, 10.5°N. Triangle indicates the relative location (130°E, 10.5°N).

the NEUC at the depth of 358 m flows eastward from the coast with its axis moving southward slightly. Afterward, it collides with the bottom topography in the vicinity of Yap Islands ( $\sim 138^\circ\text{E}$ ,  $9.5^\circ\text{N}$ ).

As shown in the latitude-depth section of  $U$  averaged over  $130^\circ\text{E}$ – $141^\circ\text{E}$  (Figure 11), the NEC (negative velocity) is located roughly at  $7^\circ\text{N}$ – $20^\circ\text{N}$  and tilts to the north with increasing depth. The NEUC is below the NEC, and the interface between them deepens northward from 250 m at  $9^\circ\text{N}$  to 500 m at  $17^\circ\text{N}$ . Such a depth range covers most of subthermocline eddies discussed above. The meridional movement of the NEC in the western Pacific has been discussed in the past studies [e.g., Qiu and Lukas, 1996; Qu and Lukas, 2003; Kim et al., 2004; Yaremchuk and Qu, 2004; Wang and Hu, 2006; Qiu and Chen, 2010; Wu, 2013]. Note that when the NEC moves northward or southward, the accompanied meridional movement of the interface between the surface westward-flowing NEC and subsurface eastward-flowing NEUC can occur as well. Thus, the meridional movement of the NEC/NEUC or their interaction with bottom topography can contribute to the generation of subthermocline eddies in the study region. To further examine this idea, we calculate the center of the NEC [Johnson et al., 2002; Hsin and Qiu, 2012a; Hsin and Qiu 2012b; Hsin et al., 2013] as follows:

$$Y_{CM}(x, t) = \frac{\int_{z=500}^{z=0} \int_{Y_S}^{Y_N} y \cdot U(x, y, z, t) dy dz}{\int_{z=500}^{z=0} \int_{Y_S}^{Y_N} U(x, y, z, t) dy dz}, \quad (2)$$

where  $Y_{CM}$  denotes the position of the NEC center in degrees,  $Y_N$  and  $Y_S$  are the northern and southern limits of integration, and  $U$  is the zonal velocity and set to zero for the positive  $U$  because the NEC is thought of as a westward flow. According to the vertical profile of the zonal velocity averaged over  $130^\circ\text{E}$ – $141^\circ\text{E}$  (Figure 11), the lower integral limit is chosen as 500 m where the deepest of the NEC bottom roughly reaches.

With setting  $Y_N = 20^\circ\text{N}$  and  $Y_S = 7^\circ\text{N}$ , Figure 12a displays the variance-preserving spectra of  $Y_{CM}$  averaged in  $130^\circ\text{E}$ – $136^\circ\text{E}$ . The spectrum peaks significantly at about 70 days, agreeing well with the

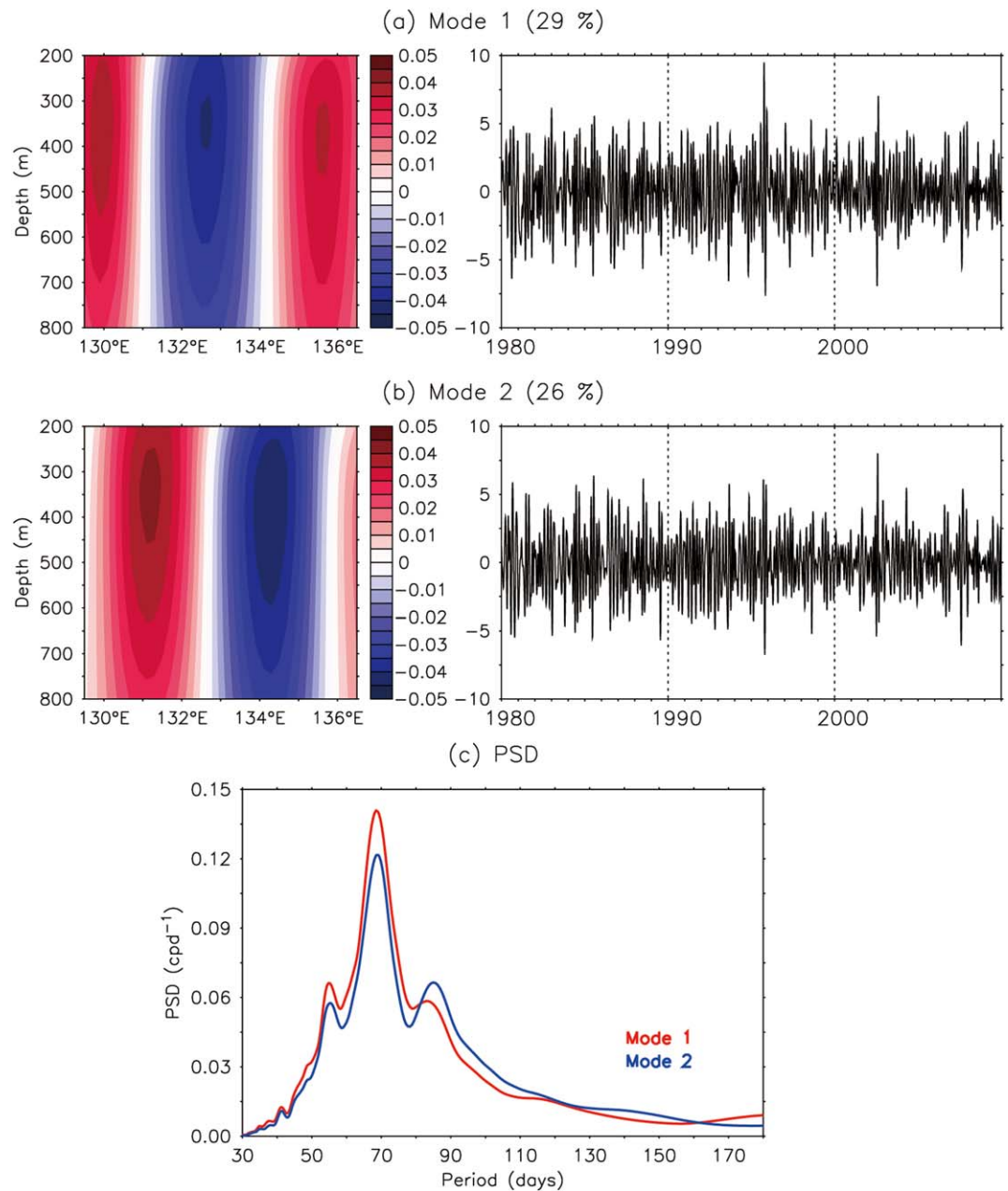


**Figure 9.** Spatial patterns and corresponding time series of (a) the first EOF mode and (b) the second EOF mode computed from the V at 10.5°N in 129°E–137°E. (c) PSD of the first and second principal components of the EOF.

spectral analyses of V in Figure 5. For clarity, we recalculate  $Y_{CM}$  by shifting  $Y_5$  from 7°N to 13°N to exclude the influence of these eddies along 10.5°N themselves. The signal is still evident (Figure 12b). Aside from these high frequency signals, the annual signal becomes significant when effects of the subthermocline eddy are removed. The variations of  $Y_{CM}$  ( $Y_N=20^\circ\text{N}$  and  $Y_S=13^\circ\text{N}$ ) at 136°E without subthermocline eddies seem to be negatively correlated with the RV at 358 m averaged over 134°E–137°E and 9°N–12°N (Figure 12c). Although their correlation coefficient is low ( $-0.1$ , 99% significance level = 0.04), to trace event by event, a negative (positive) vorticity takes place when the NEC moves to the north (south).

The NEC is the upper and northern boundaries of the NEUC in the vertical and horizontal planes, respectively (Figures 10 and 11). Combining effects of the NEC, the NEUC, and bottom topography, we

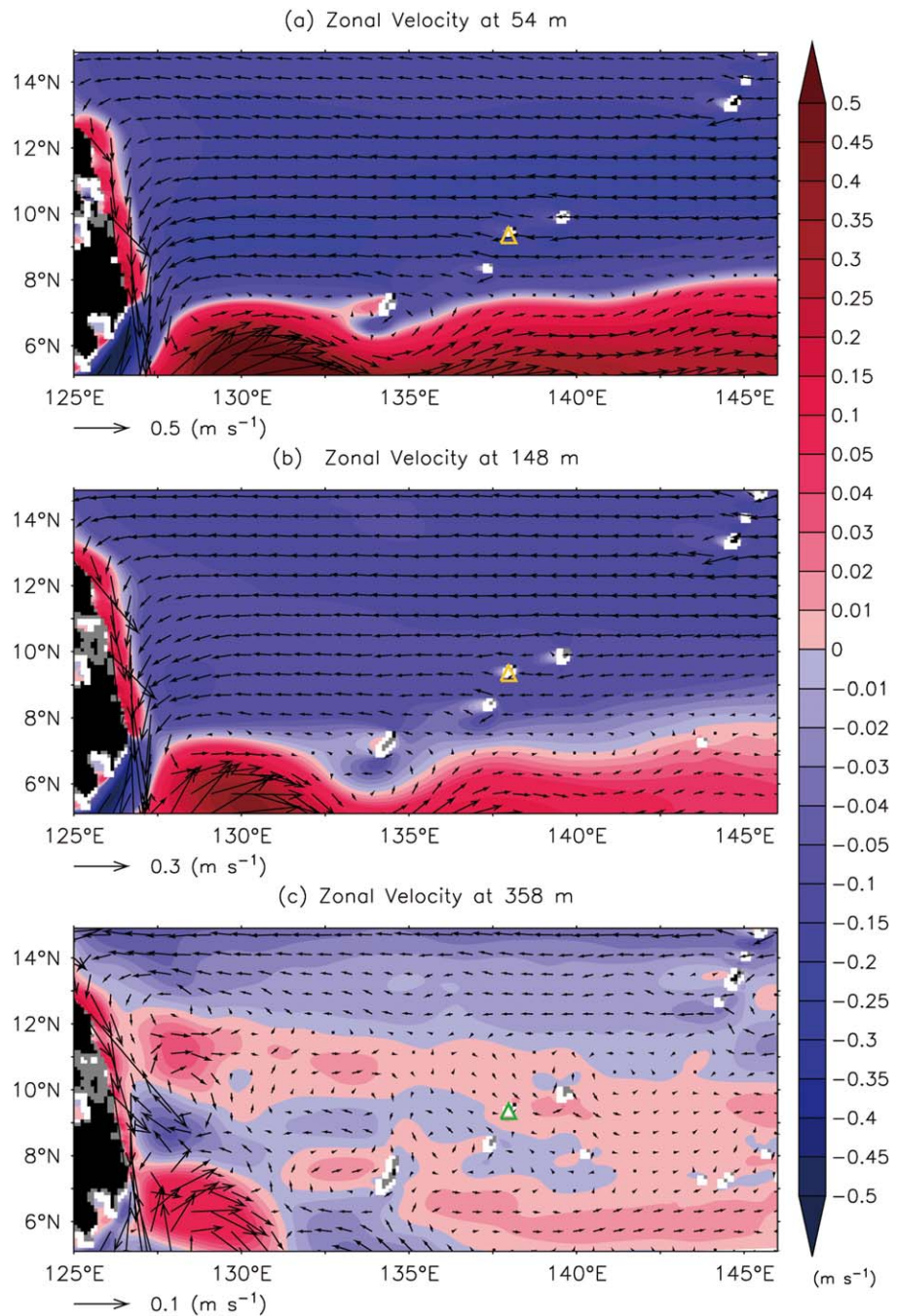


**Figure 10.** Mean zonal velocity ( $U$ , shading) and flow (vectors) patterns at the depths of (a) 54, (b) 148, and (c) 358 m. Area with depth shallower than the depth of each plot is shaded as gray color and that above the sea level is shaded by black color. The Yap Islands is denoted by triangle ( $\sim 138^\circ\text{E}$ ,  $9.5^\circ\text{N}$ ).

hypothesize that, in the barotropic point-of-view, when the subsurface NEC moves to the north, an anticyclonic (clockwise) subthermocline eddy with negative vorticity is shaded by the subsurface eastward-flowing NEUC near the Yap Islands (Figure 13a). In contrary, when the subsurface NEC moves to the south, a cyclonic (anticlockwise) subthermocline eddy with positive vorticity is generated by the subsurface westward-flowing NEC near the Yap Islands (Figure 13b). The composite subsurface depth-averaged (300–500 m) flow fields for the cases of the northernmost and southernmost locations of the NEC (Figures 13c–13f) support this hypothesis. The events with  $Y_{CM}$  larger/smaller than mean  $+1/-1$  STD are adopted for the composite of the northernmost/southernmost NEC case. As demonstrated again in this figure, a cyclonic/

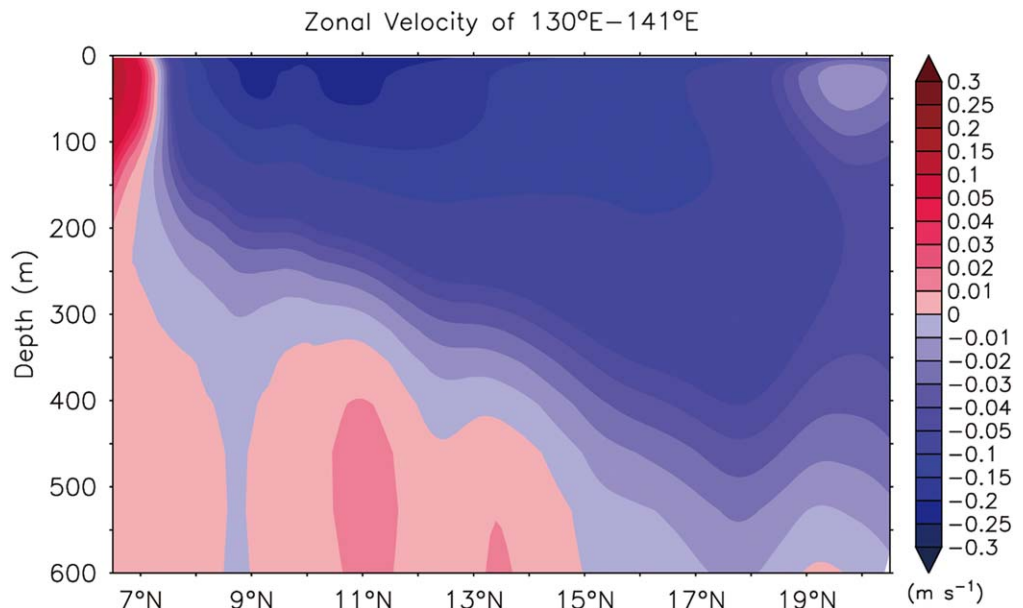


Figure 11. Latitude-depth section of zonal velocity averaged over the longitudes of 130°E–141°E.

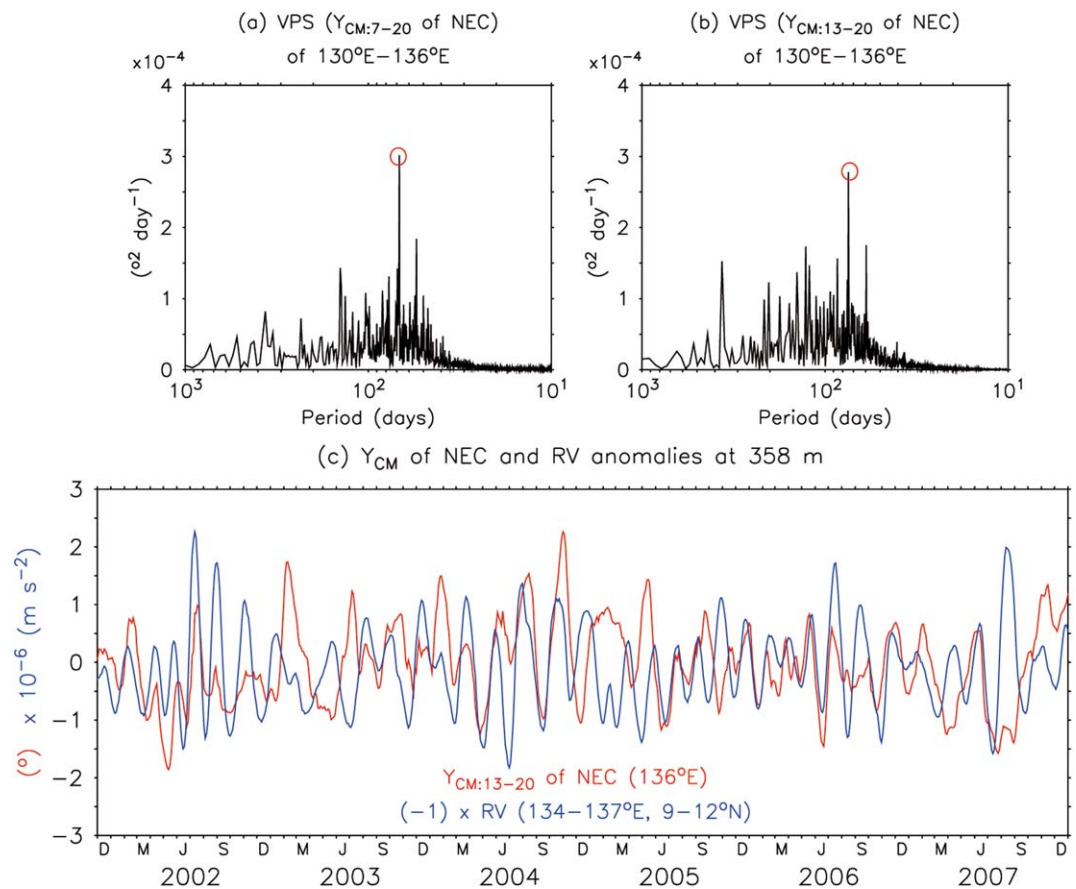
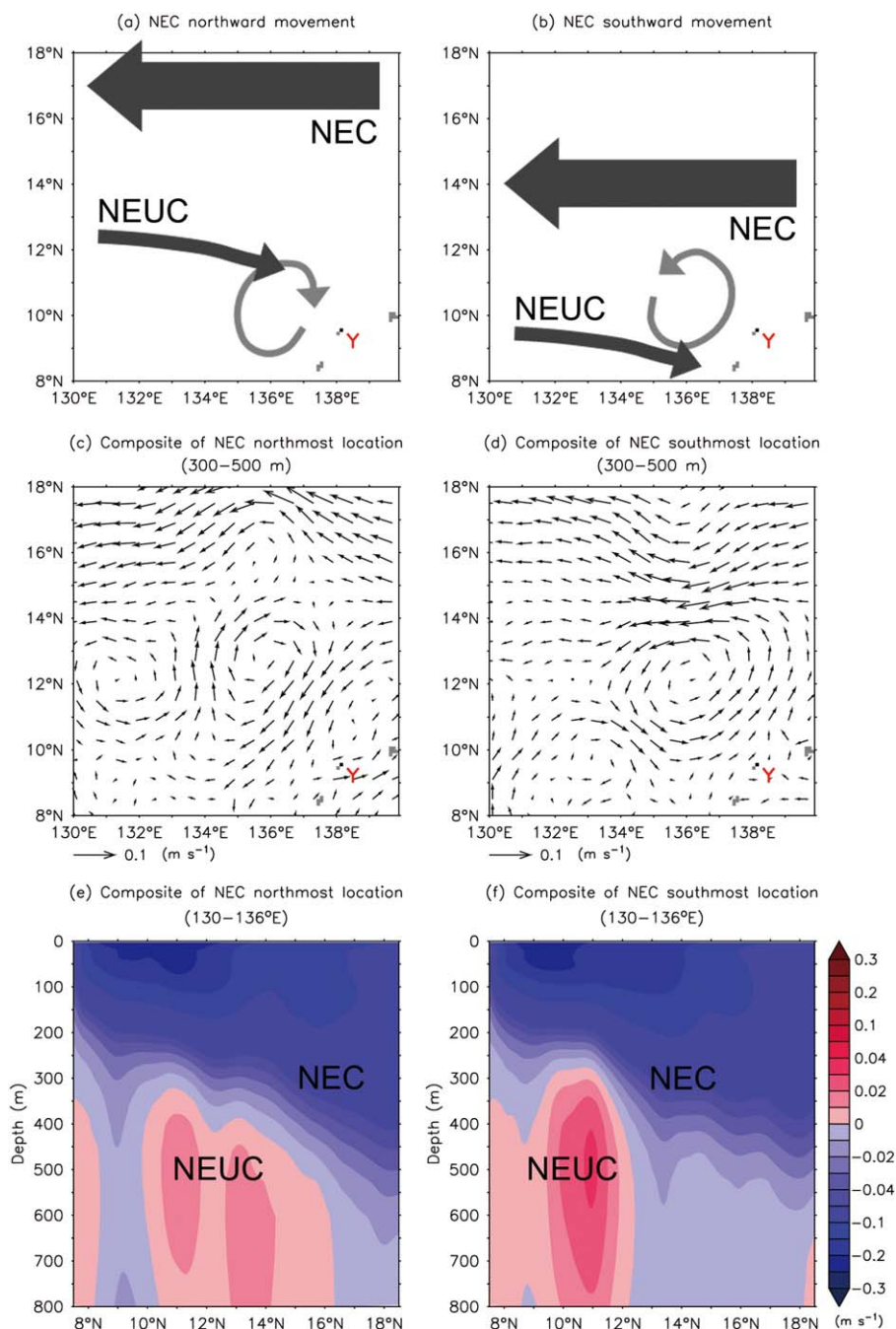


Figure 12. Variance-preserving spectra of central position ( $Y_{CM}$ ) of the North Equatorial Current (NEC) integrated meridionally in (a) 7°N–20°N and (b) 13°N–20°N averaged over 130°E–136°E. (c) Time series of NEC- $Y_{CM}$  (integrated in 13°N–20°N) at 136°E and relative vorticity (RV; averaged over 134°E–137°E, 9°N–12°N) anomalies at the depth of 358m.



**Figure 13.** Schemata of the circulation pattern for the NEC with (a) northern and (b) southern positions. Composite depth-averaged (300–500 m)/longitude-average (130°E–136°E) flow fields for the cases of the northernmost (c)/(e) and southernmost (d)/(f) locations of the NEC. Area with depth shallower than 358 m isobath is shaded as gray color and that above the sea level is shaded by black color. The Yap Islands is denoted by red Y. In Figures 13a and 13b, eddy is represented by gray arrow.

anticyclonic eddy exists west of Yap Islands, while the subsurface NEC and NEUC move to their northernmost/southernmost positions.

On the other hand, a low correlation coefficient between  $Y_{CM}$  (excluding subthermocline eddies) and the RV at 358 m averaged over 134°E–137°E and 9°N–12°N implies that not only the barotropic effect but the baroclinic effect may play a role in the generation of subthermocline eddies. In the Pacific STCC area, *Qiu and Chen* [2010] suggested that the increased eddy activities along the STCC band are due to the

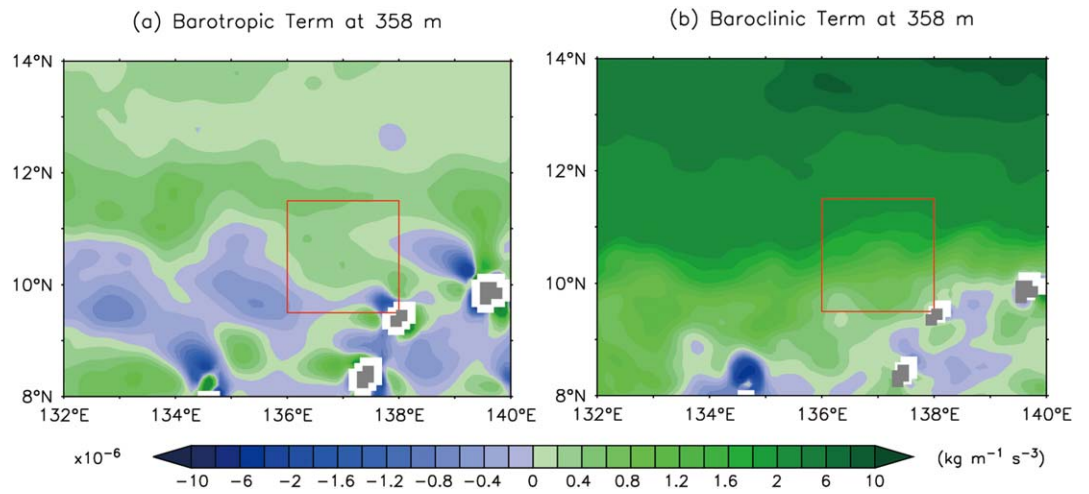


**Figure 14.** Horizontal patterns of time mean (a) barotropic conversion and (b) baroclinic conversion at 358 m. Area with depth shallower than the depth of each plot is depicted as gray shading. Red rectangle indicates the formation region of eddies.

enhanced baroclinic instability resulting from the larger vertical shear in the STCC-NEC's background flow. Thus, the vertical shear between the surface NEC and subsurface NEUC may also induce the baroclinic instability near the Yap Islands and further generate eddies in the subthermocline. Based on the analyses of Figures 6 and 7, and barotropic/baroclinic conversion in the red frame in Figure 14, we find that the formation region ( $\sim 137^\circ\text{E}$ ,  $\sim 10.5^\circ\text{N}$ ) of subthermocline eddies is dynamic equilibrium both barotropically and baroclinically, suggesting that the barotropic and baroclinic instabilities are the energy source of these eddies.

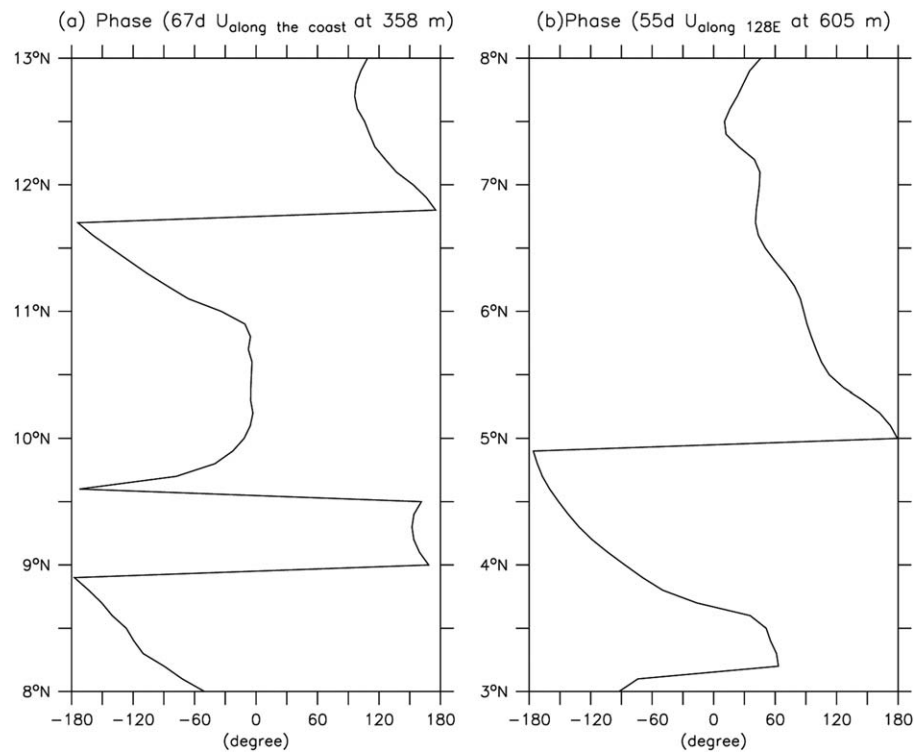


**Figure 15.** The latitudinal phase distributions of (a)  $U$  along the coast (the dashed line in Figure 3e) on the period of 67 days at 358 m and (b)  $U$  along  $128^\circ\text{E}$  on the period of 55 days at 605 m.

**Table 1.** Explained Variance of Mean Relative Vorticity ( $3^\circ$  Away From the Coast,  $9^\circ\text{N}$ – $12^\circ\text{N}$ , 358–605 m)

Intraseasonal		
30–150 Days 40.4%	50–60 Day Band Passed 3.2%	62–72 Day Band Passed 5.8%

## 5. Summary and Discussion

In this study, we investigate subthermocline eddy activities off east Philippines by analyzing results of an eddy-resolving OGCM, which has been vali-

dated in the subthermocline. There are at least two groups of eddies active in the region studied: one is from the southeast, and another is from the east. The dominant period and principal depth of the former (latter) are 50–60 days (62–72 days) and  $\sim 600$  m (300–400 m), respectively. The two groups of subthermocline eddies have similar propagation speed of  $0.12$ – $0.13$   $\text{m s}^{-1}$  and radius of  $\sim 150$  km. We suggest that the generation of subthermocline westward propagating eddies is due to the meridional movements of the westward-flowing NEC at the surface and the eastward-flowing NEUC in the subthermocline, and their interactions with topography.

The low-salinity, high oxygen features near the Philippine coast were observed by Reid [1965]. Qu *et al.* [2012] suggested that the eddy-induced fresh water flux is greater than the mean-current-induced one in the density range between  $26.9$  and  $27.3$   $\text{kg m}^{-3}$  off the Mindanao. The ensemble of eddies in this density range can significantly enhance the northward property flux. When a westward eddy collides with the coast, it can naturally move either northward or southward. However, as the result of the northwest-southeast orientation of coastline around  $10.5^\circ\text{N}$ , it seems easier for the eddy to move north-northwestward than south-southeastward. The south-southeastward eddies, if any, may be confined along the coast and decay in a very short distance due to the eastward propagating and frictional effect of topography. However, not only the 67 day south-southeastward signal but also the 67 day north-northwestward signal will decay (Figure 15a). The north-northwestward eddies (from  $10.5^\circ$  to  $12.8^\circ$ ; the distance is about  $2.3^\circ$ ) vanish more slowly than the south-southeastward eddies (from  $10.5^\circ$  to  $9.3^\circ$ ; the distance is about  $1.2^\circ$ ). In addition, the 55 day northward propagating eddies can only reach about  $7.5^\circ\text{N}$  (Figure 15b). Thus, the northward fresh water flux should be accumulated influences by many eddies of different periods (not eddies with a specific or designated period).

Table 1 shows the explained variance of mean 358–605 m RV averaged over box in  $9$ – $12^\circ\text{N}$  and  $3^\circ$  away from the coast (the dashed frame in Figure 3). As expected, the variation of RV is dominated by the intraseasonal fluctuations of 30–150 days ( $\sim 40\%$ ). The variance (9%) of the 67 day and 55 day signals accounts for  $> 20\%$  of total variance explained by intraseasonal fluctuations. The contribution of the 62–72 day signal (5.8%) is about 2 times larger than that of the 50–60 day signal (3.2%). This result suggests that the westward propagating subthermocline eddies ( $\sim 10.5^\circ\text{N}$ ) play a more important role in regulating the subsurface circulation near the Philippine coast from  $9^\circ$  to  $12^\circ\text{N}$  than those from the south. Figure 15 lends a further support for the greater impact of westward propagating subthermocline eddies on the Philippine coast. This result is similar to the analysis of Wang *et al.* [2014] that eddies on the periods of 30–90 days at 400–800 m from the region of  $9^\circ\text{N}$ – $14^\circ\text{N}$  contribute more than those from the region of  $2^\circ\text{N}$ – $9^\circ\text{N}$  to the intraseasonal variability at  $127^\circ\text{E}$ ,  $8^\circ\text{N}$ . Note that, on the timescale of 30–150 days, about 67% variance comes from the fluctuations with periods of  $> 72$  days. This indicates that eddies on periods of  $> 72$  days could play a major role in modulating the circulation pattern, heat, and salt transports off the Philippine coast. It is worthy to further investigate the properties and formation mechanism of eddies with timescales longer than 72 days.

Aside from the properties and formation mechanism of the westward propagating eddies, one may concern the propagation mechanism of them. What we can image first is that the mechanism could be related to Rossby waves. Unfortunately, the typical propagation speed of subthermocline eddies ( $0.12$   $\text{m s}^{-1}$ ) is significantly smaller than the propagation speed of the first-mode baroclinic Rossby waves around  $10^\circ\text{N}$  ( $0.2$ – $0.3$   $\text{m s}^{-1}$ ), suggesting that these subthermocline eddies are scarcely associated with the  $\beta$ -effect. In addition, another possible factor could be the subsurface eastward-flow NEUC which may decelerate westward-propagating speed of eddies from a typical Rossby wave speed ( $\sim 0.3$   $\text{m s}^{-1}$  at  $10^\circ\text{N}$ ) to the eddy speed ( $0.13$   $\text{m s}^{-1}$ ) estimated in the study. This idea may not be valid because the NEUC has a very low velocity of  $0.02$ – $0.05$   $\text{m s}^{-1}$  [Qiu *et al.*, 2013a].

Therefore, the propagation mechanism of the westward propagating eddies off the Philippine coast needs further investigations.

### Acknowledgments

This research was supported Taiwan Ministry of Science and Technology through grant 102-2811-M-003-020, 103-2811-M-003-019, 101-2611-M-003-002-MY3, and 103-2611-M-001-003. Support for T. Qu was provided by U.S. National Science Foundation through grants OCE10-29704 and OCE11-30050. The OFES simulation (<http://www.jamstec.go.jp/esc/research/AtmOcn/ofes/index.en.html>) was conducted on the Earth Simulator under the support of JAMSTEC. The 3 day OFES data are provided by the Asian-Pacific Data-Research Center (<http://apdrc.soest.hawaii.edu/>). The authors are grateful to H. Sasaki and colleagues from the Earth Simulator for assistance in processing the OFES outputs, and to the two anonymous reviewers for their thoughtful comments on an earlier version of the manuscript. School of Ocean and Science and Technology contribution 9321, and International Pacific Research Center contribution IPRC-1112.

### References

- Bracco, A., J. Pedlosky, and R. S. Pickart (2008), Eddy formation near the west coast of Greenland, *J. Phys. Oceanogr.*, *38*(9), 1992–2002, doi:10.1175/2008JPO3669.1.
- Chiang, T.-L., and T. Qu (2013), Subthermocline eddies in the western Equatorial Pacific as shown by an eddy-resolving OGCM, *J. Phys. Oceanogr.*, *43*(7), 1241–1253, doi:10.1175/JPO-D-12-0187.1.
- Cravatte, S., W. S. Kessler, and F. Marin (2012), Intermediate zonal jets in the tropical Pacific Ocean observed by Argo Floats, *J. Phys. Oceanogr.*, *42*(9), 1475–1485, doi:10.1175/JPO-D-11-0206.1.
- Du, Y., T. Qu, G. Meyers, Y. Masumoto, and H. Sasaki (2005), Seasonal heat budget in the mixed layer of the southeastern tropical Indian Ocean in a high resolution ocean general circulation model, *J. Geophys. Res.*, *110*, C04012, doi:10.1029/2004JC002845.
- Dutrieux, P. (2009), Tropical western Pacific currents and the origin of intraseasonal variability below the thermocline, PhD thesis, 140 pp., Univ. of Hawaii at Manoa, Honolulu.
- Fine, R. A., R. Lukas, F. M. Bingham, M. J. Warner, R. H. Gammon (1994), The western equatorial Pacific: A water mass crossroads, *J. Geophys. Res.*, *99*(C12), 25063–25080, doi:10.1029/94JC02277.
- Firing, E., Y. Kashino, and P. Hacker (2005), Energetic subthermocline currents observed east of Mindanao, *Deep Sea Res. Part II*, *52*(3–4), 605–613, doi:10.1016/j.dsr2.2004.12.007.
- Hogg, A. Mc C., M. P. Meredith, J. R. Blundell, and C. Wilson (2008), Eddy heat flux in the Southern Ocean: Response to variable wind forcing, *J. Clim.*, *21*, 608–620, doi:10.1175/2007JCLI1925.1.
- Hsin, Y.-C. (2015), Multidecadal variations of the surface Kuroshio between 1950s and 2000s and its impacts on surrounding waters, *J. Geophys. Res. Oceans*, *120*, 1792–1808, doi:10.1002/2014JC010582.
- Hsin, Y.-C., and B. Qiu (2012a), Seasonal fluctuations of the surface North Equatorial Countercurrent (NECC) across the Pacific basin, *J. Geophys. Res.*, *117*, C06001, doi:10.1029/2011JC007794.
- Hsin, Y.-C., and B. Qiu (2012b), The impact of Eastern-Pacific versus Central-Pacific El Niños on the North Equatorial Countercurrent in the Pacific Ocean, *J. Geophys. Res.*, *117*, C11017, doi:10.1029/2012JC008362.
- Hsin, Y.-C., C.-R. Wu, and P.-T. Shaw (2008), Spatial and temporal variations of the Kuroshio East of Taiwan, 1982–2005: A numerical study, *J. Geophys. Res.*, *113*, C04002, doi:10.1029/2007JC004485.
- Hsin, Y.-C., B. Qiu, T.-L. Chiang, and C.-R. Wu (2013), Seasonal to interannual variations in the intensity and central position of the surface Kuroshio east of Taiwan, *J. Geophys. Res. Oceans*, *118*, 4305–4316, doi:10.1002/jgrc.20323.
- Hu, D., and M. Cui (1989), The western boundary current in the far-western Pacific Ocean, in Proceedings of Western Pacific International Meeting and Workshop on TOGA-COARE, May 24–30, 1989, Nouméa, New Caledonia, edited by J. Picaut, R. Lukas, and T. Delcroix, pp. 123–134, Inst. Fr. de Rech. Sci. pour le Dév. en Coop., Nouméa.
- Hu, D., M. Cui, T. Qu, and Y. Li (1991), A subsurface northward current off Mindanao identified by dynamic calculation, in Oceanography of Asian Marginal Seas, Elsevier Oceanography Series, edited by K. Takano, vol. 54, pp. 359–365, Elsevier, Amsterdam, doi:10.1016/S0422-9894(08)70108-9.
- Hu, D., S. Hu, L. Wu, L. Li, L. Zhang, X. Diao, Z. Chen, Y. Li, F. Wang, and D. Yuan (2013), Direct measurements of the Luzon Undercurrent, *J. Phys. Oceanogr.*, *43*(7), 1417–1425, doi:10.1175/JPO-D-12-0165.1.
- Johns, W. E., T. N. Lee, D. Zhang, R. Zantopp, C.-T. Liu, and Y. Yang (2001), The Kuroshio east of Taiwan: Moored transport observations from the WOCE PCM-1 array, *J. Phys. Oceanogr.*, *31*(4), 1031–1053, doi:10.1175/1520-0485(2001)031<1031:TKEOTM>2.0.CO;2.
- Johnson, G. C., and K. E. McTaggart (2010), Equatorial Pacific 13°C Water eddies in the eastern subtropical South Pacific Ocean, *J. Phys. Oceanogr.*, *40*(1), 226–236, doi:10.1175/2009JPO4287.1.
- Johnson, G. C., B. M. Sloyan, W. S. Kessler, and K. E. McTaggart (2002), Direct measurements of upper ocean currents and water properties across the tropical Pacific during the 1990s, *Prog. Oceanogr.*, *52*(1), 31–61, doi:10.1016/S0079-6611(02)00021-6.
- Kashino, Y., H. Watanabe, B. Herunadi, M. Aoyama, and D. Hartoyo (1999), Current variability at the Pacific entrance of the Indonesian Throughflow, *J. Geophys. Res.*, *104*(C5), 11,021–11,035, doi:10.1029/1999JC900033.
- Kashino, Y., A. Ishida, and Y. Kuroda (2005), Variability of the Mindanao Current: Mooring observation results, *Geophys. Res. Lett.*, *32*, L18611, doi:10.1029/2005GL023880.
- Kashino, Y., N. España, F. Syamsudin, K. J. Richards, T. Jensen, P. Dutrieux, and A. Ishida (2009), Observations of the North Equatorial Current, Mindanao Current, and Kuroshio current system during the 2006/07 El Niño and 2007/08 La Niña, *J. Oceanogr.*, *65*(3), 325–333, doi:10.1007/s10872-009-0030-z.
- Kashino, Y., A. Atmadipoera, Y. Kuroda, and Lukijanto (2013), Observed features of the Halmahera and Mindanao Eddies, *J. Geophys. Res. Oceans*, *118*, 6543–6560, doi:10.1002/2013JC009207.
- Kim, Y. Y., T. Qu, T. Jensen, T. Miyama, H. Mitsudera, H.-W. Kang, and A. Ishida (2004), Seasonal and interannual variations of the North Equatorial Current bifurcation in a high-resolution OGCM, *J. Geophys. Res.*, *109*, C03040, doi:10.1029/2003JC002013.
- Lukas, R., E. Firing, P. Hacker, P. L. Richardson, C. A. Collins, R. Fine, and R. Gammon (1991), Observations of the Mindanao Current during the Western Equatorial Pacific Ocean Circulation Study, *J. Geophys. Res.*, *96*(C4), 7089–7104, doi:10.1029/91JC00062.
- Masumoto, Y., et al. (2004), A fifty-year eddy-resolving simulation of the world ocean: Preliminary outcomes of OFES (OGCM for the Earth Simulator), *J. Earth Simul.*, *1*, 35–56.
- Nakamura, M., and T. Kagimoto (2006), Potential vorticity and eddy potential enstrophy in the North Atlantic Ocean simulated by a global eddy-resolving model, *Dyn. Atmos. Ocean*, *41*(1), 28–59, doi:10.1016/j.dynatmoce.2005.10.002.
- Nitani, H. (1972), Beginning of the Kuroshio. in *Kuroshio: Its Physical Aspects*, edited by H. Stommel and K. Yoshida, pp. 129–163, Univ. of Tokyo Press, Tokyo.
- Qiu, B. (1999), Seasonal Eddy Field Modulation of the North Pacific Subtropical Countercurrent: TOPEX/Poseidon observations and theory, *J. Phys. Oceanogr.*, *29*(10), 2471–2486, doi:10.1175/1520-0485(1999)029<2471:SEFMOT>2.0.CO;2.
- Qiu, B., and T. M. Joyce (1992), Interannual variability in the mid- and low-latitude Western North Pacific, *J. Phys. Oceanogr.*, *22*(9), 1062–1079, doi:10.1175/1520-0485(1992)022<1062:IVITMA>2.0.CO;2.
- Qiu, B., and R. Lukas (1996), Seasonal and interannual variability of the North Equatorial Current, the Mindanao Current and the Kuroshio along the Pacific western boundary. *J. Geophys. Res.*, *101*(C5), 12,315–12,330, doi:10.1029/95JC03204.

- Qiu, B., and S. Chen (2010), Interannual-to-Decadal variability in the bifurcation of the North Equatorial Current off the Philippines, *J. Phys. Oceanogr.*, *40*(11), 2525–2538, doi:10.1175/2010JPO4462.1.
- Qiu, B., S. Chen, and H. Sasaki (2013a), Generation of the North Equatorial Undercurrent Jets by triad baroclinic Rossby wave interactions, *J. Phys. Oceanogr.*, *43*(12), 2683–2698, doi:10.1175/JPO-D-13-099.1.
- Qiu, B., D. L. Rudnick, S. Chen, and Y. Kashino (2013b), Quasi-stationary North Equatorial Undercurrent jets across the tropical North Pacific Ocean, *Geophys. Res. Lett.*, *40*(10), 2183–2187, doi:10.1002/grl.50394.
- Qu, T., and R. Lukas (2003), The bifurcation of the North Equatorial Current in the Pacific, *J. Phys. Oceanogr.*, *33*(1), 5–18, doi:10.1175/1520-0485(2003)033<0005:TBOTNE>2.0.CO;2.
- Qu, T., T. Kagimoto, and T. Yamagata (1997), A subsurface countercurrent along the east coast of Luzon, *Deep Sea Res. Part I*, *44*(3), 413–423, doi:10.1016/S0967-0637(96)00121-5.
- Qu, T., H. Mitsudera, and T. Yamagata (1998), On the western boundary currents in the Philippine Sea, *J. Geophys. Res.*, *103*(C4), 7537–7548, doi:10.1029/98JC00263.
- Qu, T., H. Mitsudera, and T. Yamagata (1999), A climatology of the circulation and water mass distribution near the Philippine coast, *J. Phys. Oceanogr.*, *29*(7), 1488–1505, doi:10.1175/1520-0485(1999)029<1488:ACOTCA>2.0.CO;2.
- Qu, T., J. Gan, A. Ishida, Y. Kashino, and T. Tozuka (2008), Semiannual variation in the western tropical Pacific Ocean, *Geophys. Res. Lett.*, *35*, L16602, doi:10.1029/2008GL035058.
- Qu, T., T.-L. Chiang, C.-R. Wu, P. Dutrieux, and D. Hu (2012), Mindanao Current/Undercurrent in an eddy-resolving GCM, *J. Geophys. Res.*, *117*, C06026, doi:10.1029/2011JC007838.
- Reid, J. L., Jr. (1965), Intermediate Waters of the Pacific Ocean, in *Johns Hopkins Oceanographic Studies*, vol. 2, 85 pp., Johns Hopkins Univ. Press, Baltimore, Md.
- Richardson, P. L., A. S. Bower, and W. Zenk (2000), A census of Meddies tracked by floats, *Prog. Oceanogr.*, *45*(2), 209–250, doi:10.1016/S0079-6611(99)00053-1.
- Roemmich, D., and J. Gilson (2001), Eddy transport of heat and thermocline waters in the North Pacific: A key to interannual/decadal climate variability?, *J. Phys. Oceanogr.*, *31*(3), 675–687, doi:10.1175/1520-0485(2001)031<0675:ETOHAT>2.0.CO;2.
- Sasai, Y., A. Ishida, Y. Yamanaka, and H. Sasaki (2004), Chlorofluorocarbons in a global ocean eddy-resolving OGCM: Pathway and formation of Antarctic Bottom Water, *Geophys. Res. Lett.*, *31*, L12305, doi:10.1029/2004GL019895.
- Sasaki, H., M. Nonaka, Y. Masumoto, Y. Sasai, H. Uehara, and H. Sakuma (2008), An eddy-resolving hindcasts simulation of the quasiglobal ocean from 1950 to 2003 on the Earth Simulator, in *High Resolution Numerical Modelling of the Atmosphere and Ocean*, edited by K. Hamilton and W. Ohfuchi, pp. 157–185, Springer, N. Y., doi:10.1007/978-0-387-49791-4\_10.
- Shapiro, G. I., and S. L. Meschanov (1991), Distribution and spreading of Red Sea Water and salt lens formation in the northwest Indian Ocean, *Deep Sea Res., Part A*, *38*(1), 21–34, doi:10.1016/0198-0149(91)90052-H.
- Simpson, J. J., and R. J. Lynn (1990), A mesoscale eddy dipole in the offshore California Current, *J. Geophys. Res.*, *95*(C8), 13,009–13,022, doi:10.1029/JC095iC08p13009.
- Toole, J., R. C. Millard, Z. Wang, and S. Pu (1990), Observations of the Pacific North Equatorial Current bifurcation at the Philippine coast, *J. Phys. Oceanogr.*, *20*(2), 307–318, doi:10.1175/1520-0485(1990)020<0307:OOTPNE>2.0.CO;2.
- Wang, Q., and D. Hu (2006), Bifurcation of the North Equatorial Current derived from altimetry in the Pacific Ocean, *J. Hydrodyn., Ser. B*, *18*(5), 620–626, doi:10.1016/S1001-6058(06)60144-3.
- Wang, Q., F. Zhai, F. Wang, and D. Hu (2014), Intraseasonal variability of the subthermocline current east of Mindanao, *J. Geophys. Res. Oceans*, *119*, 8552–8566, doi:10.1002/2014JC010343.
- Wijffels, S., E. Firing, and J. Toole (1995), The mean structure and variability of the Mindanao Current at 8°N, *J. Geophys. Res.*, *100*(C9), 18,421–18,435, doi:10.1029/95JC01347.
- Wu, C.-R. (2013), Interannual modulation of the Pacific Decadal Oscillation (PDO) on the low-latitude western North Pacific, *Prog. Oceanogr.*, *110*, 49–59, doi:10.1016/j.pocean.2012.12.001.
- Wyrtki, K. (1961), *Physical oceanography of the Southeast Asian waters*, vol. 2, NAGA report, 195 pp., Univ. of California, San Diego, Calif.
- Yaremchuk, M., and T. Qu (2004), Seasonal variability of the large-scale currents near the coast of the Philippines, *J. Phys. Oceanogr.*, *34*(4), 844–855, doi:10.1175/1520-0485(2004)034<0844:SVOTLC>2.0.CO;2.
- Zhang, L., D. Hu, S. Hu, F. Wang, F. Wang, and D. Yuan (2014), Mindanao Current/Undercurrent measured by a subsurface mooring, *J. Geophys. Res. Oceans*, *119*, 3617–3628, doi:10.1002/2013JC009693.